Journal of Materials Chemistry

Cite this: *J. Mater. Chem.*, 2012, **22**, 8566

www.rsc.org/materials

PAPER

Self-assembling PVA-F127 thermosensitive nanocarriers with highly sensitive magnetically-triggered drug release for epilepsy therapy *in vivo*†

Hsin-Yang Huang,[a] Shang-Hsiu Hu,[a] Chih-Shang Chian,[a] San-Yuan Chen,*[a] Hsin-Yi Lai[a] and You-Yin Chen*[b]

Received 3rd January 2012, Accepted 21st February 2012
DOI: 10.1039/c2jm00032f

Self-assembling, crosslinker-free, highly thermosensitive nanocarriers (TSNCs) were synthesized by the incorporation of iron oxide nanoparticles and hydrophobic drug molecules into a thermosensitive matrix composed of PEO-PPO-PEO (F127) triblock-copolymer and polyvinyl alcohol (PVA) using a mini-emulsion process. The addition of PVA significantly contributes to the stability of the thermosensitive PVA-F127 nanocarriers and reduces drug leakage because it provides hydrogen bonds to react with the PEO segments in the shell. The TSNCs exhibit a remarkable triggered size contraction and shrinkage as a result of opposing polymer thermal effects. These effects include thermal expansion of the PVA and thermal shrinkage of the F127 when the magnetic field induced a temperature change that reached 40 to 50 °C through heat generation of the magnetic nanoparticles. Depending on the PVA/F127 ratios, the TSNCs can act as a remotely triggered drug delivery platform with a tunable burst drug release profile through the structure deformation by an external magnetic field. Furthermore, the TSNCs also presented ultrasensitive magnetic resonance imaging (MRI), as demonstrated by a relatively high r_2/r_1 ratio (430). A preliminary *in vivo* study using the Long–Evans rat model has demonstrated a significant reduction in the spike-wave discharge after the anti-epilepsy drug, ethosuximide (ETX), was burst released from the TSNCs. These results were compared to PVA nanocarriers under the same magnetic induction as the *in vitro* carriers. Using a well-controlled burst release, these nanocarriers may provide significant advantages as highly temperature-responsive nanocarriers for the treatment of acute diseases.

1. Introduction

The design of a novel drug delivery system for specific disease treatments has been a technically and pharmaceutically important objective that has received increased attention worldwide. In particular, the development of multifunctional and biocompatible nanocarriers with immediately triggered release in real time is of considerable interest for the treatment of acute cerebral diseases (epilepsy and neuropathic pain) because most present drug delivery systems rely on diffusion and small delivery volumes, with complete release achieved over a few hours. Many studies have reported controlled drug release systems with material responses to stimuli such as changes in pH,[1,2] magnetic field,[3,4] electronic field,[5] ultrasound,[6,7] and temperature.[8,9] However, real-time release from a short stimulus is also hard to achieve for traditional stimuli-responsive polymeric materials,[8,9] but real-time release is critical for certain clinical complications. The practical development of a desired drug carrier should be responsive to the stimuli in real-time when an urgent need is required for disease control. Furthermore, magnetic field treatment is a non-contact method, which remotely permits the rapid trigger of the drug release action because of the heat generated by magnetic nanoparticles in comparison to those requiring physical or chemical contact. The limitations of the release rate by a magnetic field can be improved by adding thermosensitive polymers to form a magnetic-thermally sensitive release system because the system can cause strong volume deformations to release drugs as the temperature changes. A detailed review on temperature-responsive nanoparticles with embedded metal oxides to combine thermal sensitivity with magnetic signatures has been reported by Liu *et al.*[10] Recently, Hoare *et al.*[11] reported magnetically triggered nanocomposite membranes based on thermosensitive, poly(*N*-isopropylacrylamide)-based nanogels and magnetite nanoparticles to achieve "on-demand" drug delivery with an oscillating magnetic field. However, the drug release rate was too slow to apply to acute diseases because it was dependent on diffusion instead of burst release. Most recently, advances in nanotechnology show that magnetic nanoparticles

[a]*Department of Materials Science and Engineering, National Chiao Tung University, No. 1001, Ta-Hsueh Rd., Hsinchu, Taiwan 300, R.O.C. E-mail: sanyuanchen@mail.nctu.edu.tw*
[b]*Department of Biomedical Engineering, National Yang Ming University, No.155, Sec. 2, Linong St., Taipei, Taiwan 112, R.O.C. E-mail: irradiance@so-net.net.tw*

† Electronic supplementary information (ESI) available. See DOI: 10.1039/c2jm00032f

can be heated with a high frequency alternating current (AC) magnetic field, and several researchers have taken interest in magnetically triggered release. Sanson *et al.* demonstrated the feasibility of controlled drug release by radio frequency magnetic hyperthermia and showed the viability of the concept of magneto-chemotherapy with efficient multifunctional nanocarriers for combined therapy and imaging.[12] A recent study reported by Pradhan *et al.* described thermosensitive magnetic liposomes that were designed to combine features of biological and physical (magnetic) drug targeting for use in magnetic hyperthermia-triggered drug release to treat by thermo-chemotherapy in cancers.[13] Thomas *et al.* proposed newly designed inorganic porous drug nanocarriers with molecular valves as capping molecules to keep the drug inside; $(Zn_{0.4}Fe_{0.6})Fe_2O_4$ nanoparticles were incorporated inside to generate heat and build pressure inside the porous nanoparticles for the rapid removal of the molecular valves and the release of the cargo.[14] Multifunctional nanocarriers with combined rapid thermal and magnetic responses are required when a magnetic metal oxide is embedded in a temperature-responsive polymer matrix to form highly thermosensitive drug nanocarriers. Such nanosized construction displays the desirable features of an extremely fast thermal response time, enhanced magnetic susceptibility and robust drug release on demand. Using thermally sensitive polymers, Choi *et al.*[15] reported Pluronic/heparin nanocapsules that exhibited a reversible (1000 fold) volume transition. This study built on the well-known properties of poly(ethylene oxide)-poly(propylene oxide)-poly(ethylene oxide) (PEO-PPO-PEO) triblock polymers (biocompatible and commercially known as Pluronic®) that manifest a range of critical micellization temperatures (CMT) for volume/hydrophobicity transitions.

The PEO-PPO-PEO triblock copolymer, which possesses hydrophilic segments of PEO and is also known as PEG,[16] is frequently present as a biocompatible hydrophilic coating on nanoparticles to improve their *in vivo* circulation.[17,18] PPO, however, is more hydrophobic. Pluronic F127 also plays an important role in controlled drug release because of its outstanding thermal response. The structure of the Pluronic® series varies with temperature and displays structural instability with decreasing temperature below its lower critical solution temperature (LCST). Above the LCST, interchain aggregation occurs, forming alternating PEO and PPO layers arranged into micelles (with a hydrophobic PPO core and a hydrophilic PEO shell), cylinders, lamellas or other supramolecular structures. In this sense, the LCST also represents the critical micellization temperature (CMT). These colloids dilate below the LCST and shrink above the LCST. Therefore, a post-formation crosslinking agent is usually added to stabilize the supramolecular structures of PEO-PPO-PEO for synthesis of the nanocarriers or nanoparticles. Otherwise, the structure would become unstable after administration to animals, and it would be difficult to achieve *in situ* controlled drug release under an applied magnetic field to generate heat, which induces a larger change in volume, triggering drug release. Most chemical crosslinking agents are highly toxic and should be avoided. It is critical to develop a novel, crosslinker-free, temperature-responsive nanocarrier with controllable drug release that is suitable for use in the human body.

Drug leakage may occur from drug carriers synthesized using micelles with a PPO core and a PEO corona because diffusion from the nanocarriers into the environment is virtually thermodynamically unavoidable in the presence of a drug concentration gradient. In such circumstances, it is necessary to design a novel drug delivery nanocarrier with a stable surface shell to reduce drug leakage; it must also be capable of providing remotely and rapidly triggered drug release (such as induction by magnetic fields). Herein, a novel temperature-responsive nanocarrier was designed and constructed by preparing self-assembled iron oxide (SAIO) nanoparticles with drug molecules embedded in a Pluronic PVA-F127 composite matrix without any crosslinking agent. Polyvinyl alcohol (PVA) is an amphiphilic polymer that acts as a binder that can be applied in an emulsion. Within the nanoemulsion, PVA was employed as the H-bond provider to react with the PEO segment of F127 to form an ultra-thin nanoshell for the stabilization of the carrier and the elimination of undesirable drug release before it reaches the target sites. By combining the thermal expansion of PVA with the thermal shrinkage of the temperature-responsive polymers of F127, the nanocarriers provide a resulting drug carrier with a more dynamic and efficient real-time response to immediate environmental changes. Because the superparamagnetic iron oxide nanoparticles were encapsulated inside the nanocarrier, heat could be induced by an external high-frequency magnetic field to bring about a large volume change in the thermal-sensitive nanocarrier and burst drug release in a short period of time. Through this process, the nanocarrier could immediately respond to *in vitro* magnetic stimuli and solve the slow release problem of traditional drug delivery systems.

In addition, we also used a partial seizure animal model (an easier to observe epilepsy seizure compared with an acute model) to evaluate the feasibility of this newly designed drug nanocarrier for anti-epileptic treatment and to demonstrate the *in vivo* controlled release and immediate inhibition (a large amount of drug must be released quickly) of an epilepsy seizure. Ethosuximide, chemically designated as α-ethyl-α-methyl-succinimide, is a proposed T-type Ca^{2+} channel blocker. It has been successfully employed to eliminate partial seizures and has long been used as the first-choice therapeutic agent to ameliorate clinical spike-wave discharge (SWD) occurrences. As such, ethosuximide is used in this investigation as the model drug. The developed multifunctional nanocarrier was demonstrated to be non-cytotoxic, long-circulating, magnetically guided, have a high magnetization behavior, and be ultrasensitive *via* magnetic resonance imaging (MRI) detection, as well as being able to instantly release an anti-epileptic agent under remote control.

2. Results and discussion

2.1. Synthesis of thermally sensitive nanocarriers (TSNCs)

The diagram in Fig. 1(a) illustrates that without using a crosslinking agent, it was difficult to synthesize nanocarriers with only F127 because they were unstable. Specifically, micelle-like nanocarriers could be formed at a higher synthesis temperature, but as the temperature decreased (or upon cooling), the F127 tended to redistribute into the solvent because of its highly hydrophilic properties, as reported by Cohn.[19] As mentioned

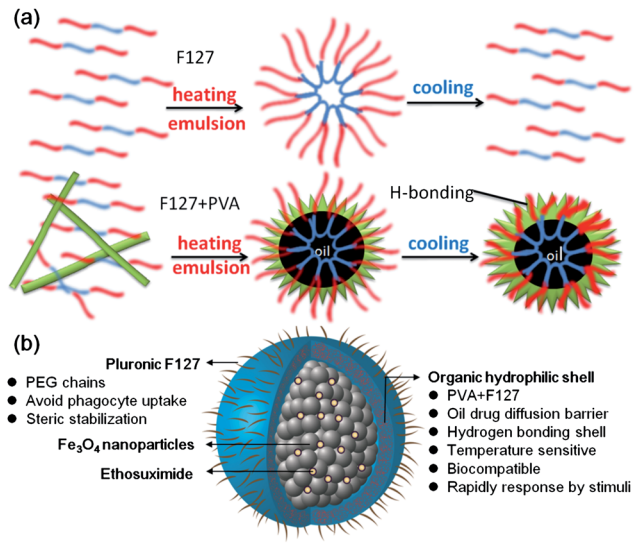

Fig. 1 Schematic representation of (a) using PVA to stabilize the F127 to form a stable nanocarrier and (b) the structure of a thermosensitive nanocarrier (TSNC) composed of PVA and F127 with iron oxide nanoparticles and drug encapsulated.

above, PVA was added as a stabilizer, and a highly stable thermosensitive PVA-F127 nanocarrier developed because the PVA provides hydrogen bonds to react with the PEO segments in the shell. These carriers exhibited a temperature response and biocompatibility. Additionally, the PEO segment of F127 can provide steric hindrance to make the nanoparticles stable as a colloidal suspension and well dispersed in aqueous solution without the need for surfactants. To achieve a rapid response, Fe_3O_4 nanoparticles were encapsulated in the nanocarriers during synthesis to trigger drug release upon exposure to magnetic stimuli. The schematic diagram in Fig. 1(b) illustrates the structure and characteristics of the thermosensitive F127-PVA nanocarriers. The Fe_3O_4 nanoparticles were used as magnetic targets, drug-releasing triggers and contrast agents for MRI analysis. PVA and Pluronic F127 are amphiphilic polymers that were assembled to synthesize the nanocarrier and encapsulate the iron oxide nanoparticles and hydrophobic drug within the core. The internal face of the nanocarrier was composed of F127 and PVA with hydrophilic PEO segments surrounding the surface, where the PEO segment end of F127 is also called PEG when exposed to a hydrophilic environment. Fig. 2(a) shows a TEM image of the PVA-F127 nanocarriers with a diameter of approximately 80 nm and iron oxide nanoparticles uniformly assembling and regularly packing inside the nanocarrier. The outer hydrophilic shell was estimated to be 5–8 nm thick and can act as a barrier to reduce inner drug release and stabilize the nanocarriers. In contrast, although pure PVA can also be assembled to form nanocarriers, without the addition of F127, no clear polymer shell can be observed on the outside of the nanocarriers, as shown in Fig. 2(b).

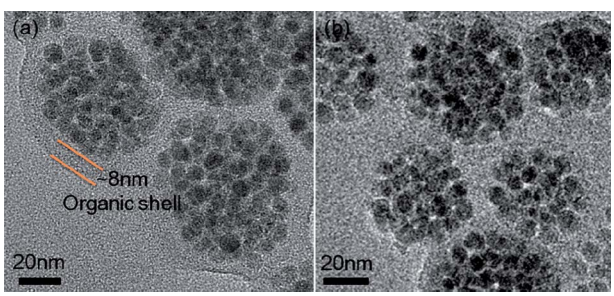

Fig. 2 Transmission electron microscopy (TEM) images of (a) thermosensitive nanocarriers of TSNC-2 (PVA/F127; 2 : 3) and (b) PVA nanocarriers. The hydrophilic polymer shell was formed on the outside of the PVA-F127 nanocarriers but not on the PVA nanocarriers.

2.2. Characterization of thermo-sensitive nanocarriers

Pluronic F127 belongs to the PEO-PPO-PEO family of triblock polymers, which manifest a range of critical micelle temperatures (CMT) or lower critical solution temperatures (LCST) for volume/hydrophobicity transitions. Pluronics are soluble below the LCST, but above that temperature, they are typically hydrophobic and do not swell in solution. The thermosensitive nanocarrier (TSNC) series synthesized from the PVA-F127 displays a characteristic LCST and is capable of displaying thermosensitive behavior similar to the PEO-PPO-PEO polymer, indicating that TSNCs exhibit a hydrophobic/hydrophilic transition. The LCST and volume change of the TSNCs can be varied through chemical modification, enabling these polymers to be tailored for diverse drug-releasing applications. To further investigate these variations, the average particle size of the TSNCs was measured by dynamic light scattering (DLS) at different temperatures. Fig. 3 shows the particle size of the TSNCs as a function of temperature, where a transition was revealed by a large change in size, depending on the relative composition ratio of PVA to F127. The average particle size of TSNC-1 (PVA/F127 = 1 : 4) was 71 nm at 25 °C, 29 nm at 40 °C and 22 nm at 45 °C as measured by DLS. The particles exhibited a 3-fold diameter transition from 25 to 45 °C. The large volume shrinkage of the TSNC-1 carriers was enough to pump the drug

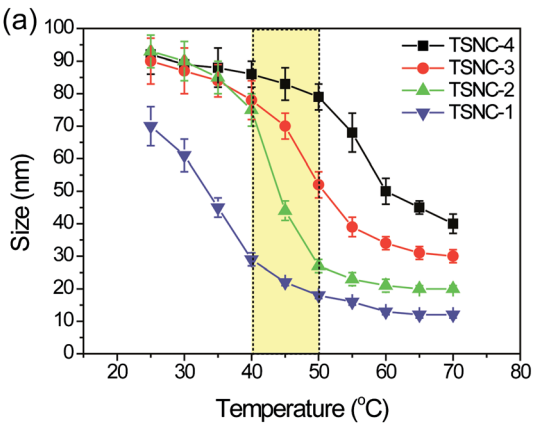

Fig. 3 The particle diameter of the PVA-F127 nanocarriers (TSNCs) was a function of the measurement temperature. The optimal application temperature in the human body should be 40 °C to 50 °C. In this temperature range, TSNC-2 would be an ideal drug delivery carrier, triggered by high frequency magnetic fields to introduce heat.

out immediately, which is attributed to the opposing thermal effect between the two polymers. With increasing PVA concentration, it was found that the LCST shifted to higher temperatures. This result was observed because PVA introduces more hydrophilic functional groups into the nanostructures, resulting in stronger interactions, such as hydrogen bonding between the PVA and F127. Furthermore, the degree of shrinkage in the nanocarriers decreased with larger additions of PVA in the TSNCs. For example, TSNC-4 with a higher PVA/F127 ratio started to shrink at a higher temperature (~50 °C) compared with the other ratios, but it presented less volume shrinkage. This result was also compounded by the interactions between PVA and F127, as mentioned in the previous paragraph. The addition of PVA results in a larger particle diameter and smaller volume shrinkage of the TSNCs above the LCST in the high temperature range; these results indicate that both the hydrophilic "swollen" state and the hydrophobic "shrunken" state appear to be constrained by the presence of PVA. The ratio of PVA/F127 in this study was an important factor. Because the TSNCs with PVA/F127 ratios of 2 : 3 to 4 : 1 remained stable after intravenous injection (LCST > 37 °C) and exhibited high-volume shrinkage and size ratios under exposure to a high-frequency magnetic field (HFMF), these TSNCs were selected to encapsulate a model drug (ethosuximide, ETX) for the treatment of epilepsy *in vivo*.

Differential scanning calorimetry (DSC) analysis was used to further investigate the hydrogen bonding interactions between the two polymers, and the results are summarized in Table 1 for various PVA/F127 ratios. When PVA was mixed with F127, the thermal behavior changed, possibly resulting from hydrogen bonds and polarity/nonpolarity repulsive forces, as measured by DSC. An endothermic peak from PVA-F127 in the heating run was detected, which was attributed to the aggregation (gel formation) of these materials (data not shown). Such aggregation is caused by the temperature sensitivity of the PPO segment. This segment can form intra- and intermolecular micelle-like aggregations due to hydrophobic interactions that reduce the inter-surface energy. Gelation started at 25.8 °C and was maximized at 28.3 °C for pure F127, but no gelation or liquefaction appeared for PVA from 10 °C to 90 °C. By increasing the PVA concentration, the LCST of the TSNCs increased from 25.8 to 45.4 °C because PVA allows for more hydrogen bonding in the nanocarriers, thus increasing the strength of the interactions between the two polymers. Therefore, TSNC-4 displayed a higher LCST in this experiment.

Table 1 Summary of PVA/F127 ratios and lower critical solution temperatures (LCSTs) of the TSNC series analyzed with differential scanning calorimetry (DSC)

	Weight ratio		
Sample	Fe_3O_4	PVA/F127	LCST
F127	1	0 : 5	25.80
TSNC-1	1	1 : 4	32.70
TSNC-2	1	2 : 3	38.01
TSNC-3	1	3 : 2	43.55
TSNC-4	1	4 : 1	47.38
PVA	1	5 : 0	None

2.3. Drug release behavior of TSNCs

The LCST of TSNC-1 was approximately 30 °C, which is lower than the temperature of the human body (37 °C). The nanocarriers cannot be used under these conditions because they will shrink when injected into an animal. Furthermore, TSNC-1 (data not shown) exhibited an apparent natural leakage due to its incompact structure at room temperature, which caused spontaneous drug release in the absence of a HFMF. Therefore, other TSNCs were used to study the drug release behavior. A magnetic field of 2.5 kA m^{-1} at a frequency of 44.2 kHz was applied to trigger the nanocarrier to release the drug. For comparison, the drug release profile of the PVA nanocarriers is also shown in Fig. 4. Fig. 4(a) displays the cumulative drug release of the PVA and PVA-F127 nanocarriers (TSNC-2, TSNC-3 and TSNC-4) in PBS at pH 7.4 without the application of a high frequency magnetic field. Although both the PVA and TSNC systems demonstrated sustained release, the drug release rates were different between the two systems. In the first 30 min, drug leakage of ETX from the PVA nanocarrier was approximately 1.54 mg mL^{-1}, but TSNC-2 showed a leakage of only 0.54 mg mL^{-1} ETX. This result indicated that TSNC-2 could remarkably reduce drug leakage compared to the PVA nanocarriers because of the stable shell. The results also suggested that the PPO chain (hydrophobic chain) can stabilize hydrophobic drugs in the core without a significant amount of leakage. As the HFMF was applied to the nanocarriers, heat could be rapidly generated to break the hydrogen bonds between the PVA and F127 and

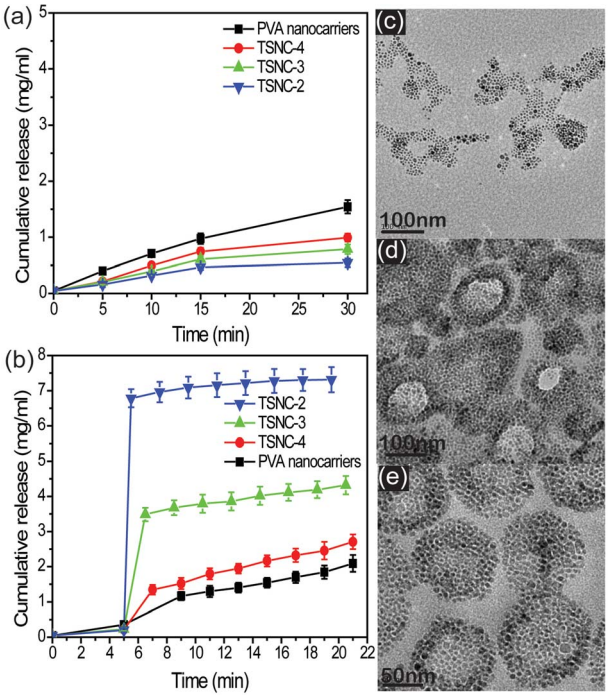

Fig. 4 (a) Comparison of drug leakage for PVA and TSNC nanocarriers. (b) Cumulative drug release profiles of ethosuximide (ETX) from PVA nanocarriers and TSNCs triggered by a high frequency magnetic field (HFMF). The TEM images of (c) TSNC-2 showed obvious ruptures and cracks and (d) TSNC-3 displayed large pores, but no obvious cracks after HFMF treatment. (e) PVA nanocarriers show nano/small cavities after applying a HFMF.

trigger drug release from the TSNCs. Fig. 4(b) shows the ETX release profiles from the TSNC carriers under magnetic fields of 2.5 kA m^{-1} at a frequency of 44.2 kHz. The results indicate that a significant acceleration in release was observed in the fifth minute during exposure to the magnetic field, which was not observed in the absence of the magnetic stimulus. For TSNC-2, the cumulative release concentration was increased from 0.4 to 6.8 mg mL^{-1} over a 30 s stimulus. It was also noted that after the removal of the magnetic field, no apparent drug release was detected, indicating that the encapsulated drug has been rapidly released. This finding suggests that the nanostructures were irreversibly deformed and ruptured, thus maintaining their rapid release rate after removal of the stimulus. As the PVA content was increased, TSNC-3 still displayed burst-like release, but the released drug decreased to 3.5 mg mL^{-1} within 90 s of exposure to the stimulus. In contrast, for the PVA nanocarriers, a very small quantity (1.2 mg mL^{-1}) was released even when exposed to the magnetic field for longer periods of time, such as 240 s. The temperature response was too low to trigger drug release. A similar phenomenon also occurred in TSNC-4, which maintained a slow drug release behavior. To further elucidate the mechanism behind the magnetically triggered release behavior, the TSNC nanocarriers were examined using HR-TEM. Fig. 4(c) clearly displays ruptures and cracks in the resulting TSNC-2 nanocarriers after exposure to a HFMF for 30 s. This evidence also suggested that the heat induced by the external magnetic field not only induced a large shrinkage in the volume of the nanocarriers but also caused disruptive changes to the structure, resulting in instantaneous drug release. For a nanocarrier with a higher PVA/F127 ratio, such as TSNC-3, it displayed a similar rapid release profile to TSNC-2 during exposure to an identical magnetic field. The cumulative release amount decreased, indicating that a higher PVA content clearly decreased the drug release response because of the reduced thermosensitivity. Fig. 4(d) shows that after exposure to the stimulus (90 s), the nanocarrier displayed a hole-like morphology as a result of a rapid volume/hydrophobicity transition of the core phase, causing irreversible pores in the shells. Without the addition of a thermosensitive polymer, the morphological structure of the as-synthesized PVA nanoparticles in the absence of HFMF treatment displayed excellent structural integrity. However, after 4 min of a HFMF stimulus, nanocavities developed in the PVA nanoparticles, but the nanoparticles remained structurally intact, as shown in Fig. 4(e).

2.4. Magnetic characterization and contrast agent relaxivity

The TSNC series appeared to be suitable as a T2-type MRI contrast enhancement agent because of its high saturation magnetization and low cytotoxicity. The magnetic properties of Fe_3O_4 nanoparticles and TSNCs were measured by SQUID at 298 K with the magnetic field sweeping from −10 000 to +10 000 G. Fig. S1(a)† shows the correlation of the magnetization with the magnetic field for the Fe_3O_4 nanoparticles and TSNC nanocarriers with various PVA/F127 ratios, where the curves show similar shapes with negligible hysteresis. A very high value of 87 emu g^{-1} was obtained for the Fe_3O_4 nanoparticles; the magnetization was very close to the theoretical value of approximately 92 emu g^{-1}.[20] Such high saturation magnetization values for the iron oxides that were synthesized can be explained by their highly crystalline character, which provides good translation efficiency from magnetic to thermal energy and a high susceptibility contrast in MR imaging. However, the presence of PVA and F127 diluted the concentration of the Fe_3O_4 nanoparticles, resulting in a lower saturation magnetization (M_s) of the TSNC nanocarriers compared with that of pure Fe_3O_4 nanoparticles. The magnetic properties of the PVA-F127 nanocarriers displayed negligible variations at different PVA/F127 ratios. In this study, TSNC-2 displayed a fast response in the drug release experiments; therefore, it was desirable to investigate its magnetic behavior and applications in other *in vivo* tests. Fig. S1(b)† shows the T_2-weighted MR images of aqueous dispersions of different TSNC-2 concentrations. The MR signal decreased with an increasing content of TSNC-2, demonstrating the efficiency of the magnetic core of TSNC-2 at enhancing the transverse (T_2) proton relaxation process. The efficacy and stability of TSNC-2 as a MR contrast agent was further evaluated by measuring the longitudinal (r_1) and transverse (r_2) relaxivities using an MR scanner. Fig. S1(c)† shows that the inverse relaxation times, $1/T_1$ and $1/T_2$, varied linearly with the iron concentration and the slope was defined as the longitudinal (r_1) and transverse (r_2) relaxivities, respectively. The r_1 and r_2 values of the synthesized TSNC-2 were measured to be 0.402 s^{-1} mM^{-1} Fe and 172.98 s^{-1} mM^{-1} Fe, respectively. The lower longitudinal relaxation could be a result of the encapsulation of Fe_3O_4 nanocrystals inside the hydrophobic PPO blocks of F127, which reduces the close contact between water molecules and the magnetic nanocrystals. The relaxivity ratio, r_2/r_1, is another important factor used to evaluate the efficiency of T_2-type contrast agents, and a larger relaxivity ratio is desirable. For TSNC-2, the r_2/r_1 ratio was calculated to be approximately 430. Therefore, TSNC-2 could perform well as a T_2-type MR contrast enhancement agent for cellular or molecular imaging and diagnostic applications.

2.5. Comparison of ETX@TSNC-2 *vs.* ETX@PVA in the treatment of epilepsy *in vivo*

As mentioned above, the response from TSNC-2 was faster than that of the other TSNCs. For comparison, PVA nanocarriers were used. For the *in vivo* experiments, rats with spontaneous absence epilepsy were used to evaluate the therapeutic effect of bulk drug release from the TSNC-2 and PVA nanocarriers. In the preliminary study, Fig. 5(a) presents 7T MR imaging (FLASH; TE = 9.2 ms, TR = 335.1 ms, SLTH = 1 mm, Flip angle = 15°, NEX = 2 and acquisition matrix 256 × 256) of the retention of the nanocarriers in the cortical and subcortical areas of the right hemisphere following the 15 min magnetic targeting. In the targeting region, the MR signal to the nanocarriers was 2–3 times lower than the contralateral hemisphere without an accumulation of nanocarriers. Fig. 5(b) displays a restrained rat that remotely received a high frequency magnetic field (HFMF) as a trigger for antiepileptic drug release to observe the thermosensitive difference between the ETX@TSNC-2 and ETX@PVA nanocarriers. While subjecting Group I (ETX@TSNC-2) to a HFMF for 15 s, lower intensities of the spike-wave discharges (SWDs) were clearly found, but a slight decrease in the SWD intensities in Group II (ETX@PVA) following a 15 sec HFMF treatment in the subsequent 2 h was

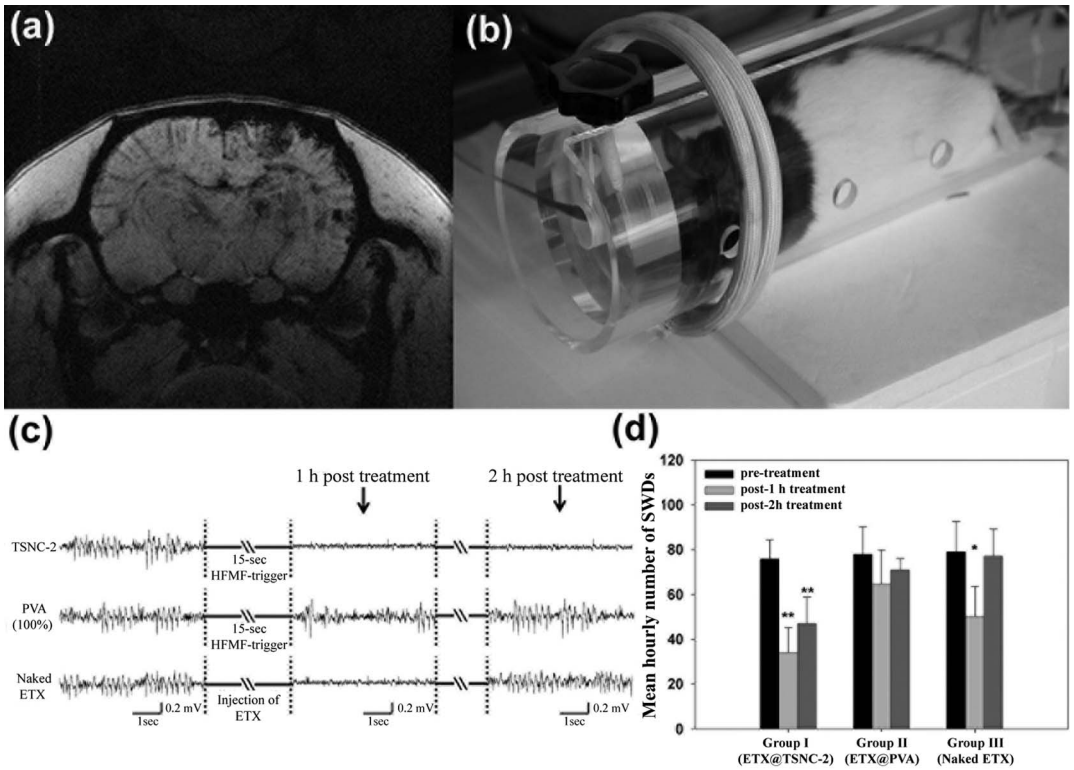

Fig. 5 Therapeutic effects of magnetically released antiepileptic drugs from the intravenous injection of nanocarriers *in vivo*. (a) 7T MR imaging of the retention of the nanocarriers in the cortical and subcortical areas of the right hemisphere following 15 min magnetic targeting. (b) The restrained animal received HFMFs to trigger drug release from the nanocarriers, and a non-magnetic multielectrode array monitored seizure activity. (c) Rats in Group I showed significant reductions of SWD occurrences after 2 h of exposure to the HFMF. However, there was no apparent reduction in SWD occurrences in Group II following HFMF treatment. There were significant decreases in the mean hourly numbers of SWDs 1 h post-injection of naked ETX, but an increase in the mean hourly numbers of SWDs was found 2 h post-injection. (d) Comparison of the mean number of SWDs for a 1 h period within Group I, Group II, and Group III pre-HFMF and post-HFMF treatment. $^{**}p < 0.01$ statistically significant decreases were present when pre-HFMF was compared to post-HFMF in Group I.

observed. The rats in Group III showed decreasing SWDs after 1 h administration of the naked ETX. However, a significant increase in the intensities of the SWDs 2 h post-treatment of the naked ETX is shown in Fig. 5(c).

Fig. 5(d) of Group I showed a statistically significant decrease in the mean hourly numbers of SWDs 1 and 2 h post-HFMF trigger ($p < 0.01$), which was comparable with those in the pre-HFMF treatment of ETX@TSNC-2, and successfully demonstrated the longer term therapeutic effect for *in vivo* applications. However, the mean hourly numbers of SWDs 1 and 2 h post-HFMF trigger in Group II compared with those for the pre-HFMF treatment of ETX@PVA nanocarriers were not significant ($p > 0.05$). There was a significant decrease ($p < 0.05$) in the mean hourly numbers of SWDs 1 h post-injection of the naked ETX. An increase in the mean hourly numbers of SWDs was found 2 h post-injection and showed insignificant differences in the non-significant mean hourly numbers of SWDs, which were compared with those in the pretreatment of naked ETX in Group III.

Because PVA is not very sensitive to temperature changes induced from magnetic stimulation, epileptic seizures of rats injected with the ETX@PVA nanocarriers were not significantly inhibited under an external magnetic field. On the contrary, epileptic episodes of rats injected with ETX@TSNC-2 were reduced by at least 60% after exposure to a magnetic field (induced by the heat machine) for 15 s because the TSNC-2 showed a highly temperature-responsive characterization. The above-mentioned results demonstrated that both the lower dose ETX@TSNC-2 and the naked ETX showed significant decreases in the number of SWDs during the first hour. However, only ETX@TSNC-2 produced an enhancement effect during the second hour, resulting in better control over absence seizures. The administration of ETX@TSNC-2 may be useful in reducing the therapeutic dose of ETX and its side effects[21–23] or may be considered for the treatment of patients with refractory absence epilepsy.

3. Experimental

The synthesis was carried out in an air-free atmosphere, and we used commercially available reagents. Absolute ethanol (99.5%), benzyl ether (99%), 1,2-hexadecanediol (97%), oleic acid (90%), oleylamine (>70%), dichloromethane (99.9%), and iron(III) acetylacetonate were purchased from Aldrich Chemical Co. Polyvinyl alcohol (PVA, M_w: 10k) was purchased from Fluka Chemical Co. Pluronic F127 was purchased from Sigma. ETX (Product No. E7138, Sigma, St. Louis, Mo, USA) was used as the model drug.

3.1 Synthesis of Fe_3O_4 nanoparticles

The monodispersed superparamagnetic iron oxide nanoparticles (Fe_3O_4) were synthesized through the high-temperature decomposition of $Fe(acac)_3$. Briefly, 10 nm of Fe_3O_4 nanoparticles were synthesized by mixing 2 mmol of $Fe(acac)_3$ (iron III acetylacetonate), 10 mmol of 1,2-dodecanediol, 6 mmol of oleic acid, 6 mmol of oleylamine, and 20 mL of benzyl ether under a flow of nitrogen. The mixture was stirred magnetically and was preheated to reflux (200 °C) for 30 min and then heated to 300 °C for another 1 h under nitrogen. The black–brown mixture was allowed to cool to room temperature and was then treated with 50 mL of ethanol to precipitate. The products were collected by centrifugation at 6000 rpm for 10 min and were then washed four times with an excess of pure ethanol. The product, Fe_3O_4 nanoparticles, was centrifuged to remove the solvent and was redispersed into ethanol.

3.2 Synthesis and drug release of ETX-loaded thermosensitive nanocarriers (TSNCs)

To prepare the thermosensitive nanocarriers, 6 mL (10 mg mL^{-1}) of iron oxide nanoparticles were centrifuged at 6000 rpm for 10 min, and were redispersed in 2 mL of dichloromethane containing 10% ETX (model drug) to form an organic phase. Next, PVA and F127 polymer solutions were prepared. One hundred milligrams of polyvinyl alcohol (PVA) was dissolved in 5 mL of deionized (DI) water and heated at 70 °C until it was completely dissolved. Pluronic F127 (150 mg) was dissolved in 5 mL of DI water. Subsequently, different ratios of PVA/F127 (Table 1) were prepared by mixing the two solutions. The organic phase was added into the polymer solution and emulsified for 5 min with a 100 W ultrasonicator. The mixture was magnetically stirred at room temperature to evaporate the organic solvent. After evaporation of the organic solvent, the drug-containing nanocarriers were washed with DI water 3 times and then separated from the aqueous solution by centrifugation at 12 000 rpm for 5 min. *In vitro* drug release from the TSNCs with various PVA/F127 ratios was evaluated by incubating the ETX-containing nanocarriers in 20 mL of PBS. At specific time intervals, 1 mL of the medium solution was taken out for concentration detection by a UV-vis spectrophotometer (8453 UV-Visible spectrophotometer, Agilent Technologies, Inc., USA) and replaced with the same volume of fresh media. The measurements were performed in triplicate.

3.3 Measurement of particle size, thermal characterization, magnetization and contrast agent relaxivity

The morphology of the TSNCs was examined using transmission electron microscopy (TEM, JEOL Ltd., Japan, JEM-2100). Dynamic light scattering (DLS, Beckman Coulter, Inc., USA, Delsa™ Nano C, Particle Analyzer) was used to determine the electrophoretic movement of charged particles under an applied electric field from the Doppler shift of scattered light, where TSNCs were measured at different temperatures from 293 K to 343 K. Differential scanning calorimetry (Perkin-Elmer, Inc., USA, PYRIS Diamond™ DSC) has been used to characterize physical mixtures prepared from commercial grades of Pluronic F127 and PVA. The polymer blends were prepared by dissolving and mixing in DI water at 298 K, and the polymer blend ratios are listed in Table 1. Samples (3 to 5 mg) were dried under vacuum for approximately 48 h and analyzed using DSC at a heating rate of 10 K min^{-1} from 283 K to 363 K. The magnetization of the nanocarriers was measured by a superconducting quantum interference device (SQUID, Quantum Design, USA, MPMS-XL7) at 298 K and ±10 000 G applied magnetic field. Before SQUID analysis, the iron oxide nanoparticles, TSNCs and PVA nanocarriers were dried in a vacuum oven at 333 K for 48 h. For the measurement of relaxivity of the iron oxide nanoparticles, MR *in vitro* assays were performed using a 7 Tesla rodent MRI scanner (BioSpec 70/30, Bruker Topspin, Ettlingen, Germany). The T_1 relaxivity (r_1) and T_2 relaxivity (r_2) were determined by diluting TSNC-2 with 0.5% agarose gel in 7 steps to concentrations of 0 to 0.001 mmol L^{-1} (corresponding Fe concentrations, 0–1.08 mmol L^{-1}). A quadrature-volume coil with an inner diameter of 112 mm was used for RF transmission and reception. The T_1 and T_2 weighted images were obtained by the multi-slice multi-echo (RARE: TE = 10.5 ms; TR = 1300 ms; SLTH = 1 mm; acquisition matrix 384 × 192; field of view (FOV) = 5.0 × 2.5 cm^2; NEX = 10) and spin echo (Turbo RARE: TE = 33 ms; TR = 2500 ms; SLTH = 1 mm; acquisition matrix 384 × 192; field of view (FOV) = 5.0 × 2.5 cm^2; NEX = 6) sequences, respectively.

3.4 Experimental animals

Long–Evans male rats (n = 18) obtained from the National Laboratory Animal Center at National Yang Ming University were raised separately at 22 ± 2 °C under rotating 12 h light/dark conditions and were given ordinary animal feed and drinking water. The animals had a mean body weight of 250–300 g. The study was approved by the Institutional Animal Care and Use Committee at the National Chiao Tung University and National Yang Ming University and conducted according to the standards established in the Guide for the Care and Use of Laboratory Long–Evans rats as an absence epilepsy model.[24] The animals were used to evaluate the therapeutic effect of drug release from the nanocarriers.

3.5 High frequency magnetic field (HFMF)-triggered drug release *in vivo*

This study was designed to investigate magnetically targeted nanocarriers and HFMF-triggered antiepileptic drug release from nanocarriers *in vivo*. Before these experiments were carried out, the rats were trained to adapt in the holder for 30 min daily, in order to decrease animal stress, for 2 weeks. In addition, to record the animals' routine brain waves,[25] we implanted a non-magnetic multielectrode array in the animal skull in advance, and then the animals were allowed a 1 week recovery period. Before magnetic targeting and HFMF, a 2 h electrophysiological recording was taken for each animal.[26] The next day, implanted animals were equally divided into three groups in this study. Group I (n = 6) and Group II (n = 6) received intravenous injections of ETX@TSNC-2 and ETX@PVA, respectively, and then both groups were subjected to magnetic targeting. Group III (n = 6) received the intraperitoneal injection of ETX (9.33 mg kg^{-1}), and the same concentration of free ETX as those

loaded on the nanocarriers, as a control for the evaluation of the effect of nanocarriers.

After the intravenous administration of nanocarriers (ETX@TSNC-2 or ETX@PVA) in Group I and II at a dose of 12 mg Fe kg^{-1}, magnetic targeting was achieved in the right hemisphere of the rat brain. The rat head was placed under a permanent magnet with a density of 0.4 T for 15 min. Following the magnetic targeting, the animal was restrained in the adapted holder, which was mounted inside a horizontal two-turn copper coil centered on the rat's head. A 15 sec HFMF at 44.2 kHz and a magnetic field strength (H) of 2.5 kA m^{-1} was applied to trigger drug release. Each animal received the electrophysiological recording for 2 h following HFMF triggering. Group III also received a 2 h electrophysiological recording following the intraperitoneal administration of naked ETX to evaluate the therapeutic effect compared to the nanocarriers.

The cumulative number of spike and wave discharges (SWDs) in a 1 h period[27] was used to compare the therapeutic effect of absence epilepsy among Group I, Group II and Group III. Statistical analysis was performed using SPSS (Statistical Package for the Social Sciences, version 10.0; SPSS, Chicago, IL, USA) for Windows. The mean hourly numbers of SWDs for 1 h pre- and post-treatment and 2 h post-treatment within a group were compared using ANOVA with a *post hoc* Tukey's test ($p < 0.05$).

Conclusions

In summary, we reported TSNCs composed of thermosensitive F127 and PVA block copolymers incorporating iron oxide nanoparticles and ETX drug molecules *via* a mini-emulsion process. The inner cores exhibited a significant triggering size contraction and shrinkage when the magnetic field induced a temperature change reaching 40 to 50 °C, making the nanocarriers collapse. Under HFMF treatment, the TSNCs are capable of delivering drugs with a fast and precise response over a wide variety of release patterns, including burst release and sustained release, depending on the PVA/F127 composition and the applied magnetic field. During the *in vivo* tests, the preliminary data showed that the nanocarriers immediately displayed a significant reduction in the spike-wave discharge during epileptic seizures by an external magnetic stimulus and also showed an ultrasensitive MRI after injection. A more extensive and in-depth *in vivo* study is under development, and the results that will be reported separately look promising.

Acknowledgements

This work was financially supported by the National Science Council of the Republic of China, Taiwan under Contract of NSC99-2221-E-009-070-MY3 and NSC100-2320-B-009-006-MY2. We also thank 7T animal MRI Core Lab of the Neurobiology and Cognitive Science Center for technical and facility support, and C. H. Hsieh and J. H. Chen of the Instrumentation Center for MRI experiments at National Taiwan University. This work is also supported by "Aim for the Top University Plan" of the National Chiao Tung University and Ministry of Education, Taiwan, R.O.C.

References

1 V. Cauda, C. Argyo, A. Schlossbauer and T. Bein, *J. Mater. Chem.*, 2010, **20**, 4305–4311.
2 M. Das, S. Mardyani, W. C. W. Chan and E. Kumacheva, *Adv. Mater.*, 2006, **18**, 80–83.
3 S.-H. Hu, D.-M. Liu, W.-L. Tung, C.-F. Liao and S.-Y. Chen, *Adv. Funct. Mater.*, 2008, **18**, 2946–2955.
4 P.-J. Chen, S.-H. Hu, C.-S. Hsiao, Y.-Y. Chen, D.-M. Liu and S.-Y. Chen, *J. Mater. Chem.*, 2011, **21**, 2535–2543.
5 K. C. Wood, N. S. Zacharia, D. J. Schmidt, S. N. Wrightman, B. J. Andaya and P. T. Hammond, *Proc. Natl. Acad. Sci. U. S. A.*, 2008, **105**, 2280–2285.
6 B. G. De Geest, A. G. Skirtach, A. A. Mamedov, A. A. Antipov, N. A. Kotov, S. C. De Smedt and G. B. Sukhorukov, *Small*, 2007, **3**, 804–808.
7 H. J. Kim, H. Matsuda, H. Zhou and I. Honma, *Adv. Mater.*, 2006, **18**, 3083–3088.
8 C. Liu, J. Guo, W. Yang, J. Hu, C. Wang and S. Fu, *J. Mater. Chem.*, 2009, **19**, 4764–4770.
9 N. S. Satarkar and J. Z. Hilt, *J. Controlled Release*, 2008, **130**, 246–251.
10 T.-Y. Liu, S.-H. Hu, D.-M. Liu, S.-Y. Chen and I. W. Chen, *Nano Today*, 2009, **4**, 52–65.
11 T. Hoare, J. Santamaria, G. F. Goya, S. Irusta, D. Lin, S. Lau, R. Padera, R. Langer and D. S. Kohane, *Nano Lett.*, 2009, **9**, 3651–3657.
12 C. Sanson, O. Diou, J. Thévenot, E. Ibarboure, A. Soum, A. Brûlet, S. Miraux, E. Thiaudière, S. Tan, A. Brisson, V. Dupuis, O. Sandre and S. b. Lecommandoux, *ACS Nano*, 2011, **5**, 1122–1140.
13 P. Pradhan, J. Giri, F. Rieken, C. Koch, O. Mykhaylyk, M. Döblinger, R. Banerjee, D. Bahadur and C. Plank, *J. Controlled Release*, 2010, **142**, 108–121.
14 C. R. Thomas, D. P. Ferris, J.-H. Lee, E. Choi, M. H. Cho, E. S. Kim, J. F. Stoddart, J.-S. Shin, J. Cheon and J. I. Zink, *J. Am. Chem. Soc.*, 2010, **132**, 10623–10625.
15 S. H. Choi, J.-H. Lee, S.-M. Choi and T. G. Park, *Langmuir*, 2006, **22**, 1758–1762.
16 R. Gref, A. Domb, P. Quellec, T. Blunk, R. H. Müller, J. M. Verbavatz and R. Langer, *Adv. Drug Delivery Rev.*, 1995, **16**, 215–233.
17 S. Stolnik, B. Daudali, A. Arien, J. Whetstone, C. R. Heald, M. C. Garnett, S. S. Davis and L. Illum, *Biochim. Biophys. Acta, Biomembr.*, 2001, **1514**, 261–279.
18 A. Besheer, J. r. Vogel, D. Glanz, J. r. Kressler, T. Groth and K. Mäder, *Mol. Pharmaceutics*, 2009, **6**, 407–415.
19 D. Cohn, H. Sagiv, A. Benyamin and G. Lando, *Biomaterials*, 2009, **30**, 3289–3296.
20 J.-P. Fortin, C. Wilhelm, J. Servais, C. Ménager, J.-C. Bacri and F. Gazeau, *J. Am. Chem. Soc.*, 2007, **129**, 2628–2635.
21 H. R. John, *Epilepsy Behav.*, 2009, **15**, 404–412.
22 E. Russo, R. Citraro, F. Scicchitano, S. De Fazio, E. D. Di Paola, A. Constanti and G. De Sarro, *Epilepsia*, 2010, **51**, 1560–1569.
23 M. Z. Gören and F. Onat, *CNS Drug Rev.*, 2007, **13**, 224–239.
24 M. A. Cortez, C. McKerlie and O. C. Snead, *Neurology*, 2001, **56**, 341–349.
25 P.-F. Yang, D.-Y. Chen, J. W. Hu, J.-H. Chen and C.-T. Yen, *Pain*, 2011, **152**, 194–203.
26 A. M. L. Coenen, W. H. I. M. Drinkenburg, B. W. M. M. Peeters, J. M. H. Vossen and E. L. J. M. van Luijtelaar, *Neurosci. Biobehav. Rev.*, 1991, **15**, 259–263.
27 O. Akman, T. Demiralp, N. Ates and F. Y. Onat, *Epilepsy Res.*, 2010, **89**, 185–193.